

INTERPOLATING CATHODE PAD READOUT IN GAS PROPORTIONAL DETECTORS FOR HIGH MULTIPLICITY PARTICLE TRACKS*

B. Yu, V. Radeka, G.C. Smith and E. O'Brien
 Brookhaven National Laboratory Upton, NY 11973

Experiments which are planned for the Superconducting Super Collider and the Relativistic Heavy Ion Collider will involve interactions in which detectors will need to identify and localize hundreds or even thousands of particle tracks simultaneously. Most types of conventional position sensitive, proportional detectors with projective geometry are not able to unravel the individual tracks in these environments. We have been investigating several forms of sub-divided cathode readout to address this problem. We report here on geometric charge division using chevron shaped cathode pads which lie in rows underneath each anode wire. Investigations have quantified the non-linear effects due to avalanche angular localization, and how these become negligible with proper design of the cathode pad. Differential non-linearity of $\pm 5\%$, and position resolution in the region of $50 \mu\text{m}$ rms, have been achieved.

1. Introduction

In many future experiments involving high energy particles and heavy ions, and also those at X-ray synchrotron sources, there will be a requirement for position sensitive detectors that work with significantly higher counting rates than at present. Experiments which are planned for the Superconducting Super Collider, and the Relativistic Heavy Ion Collider, will involve interactions in which detectors will need to identify and localize hundreds or even thousands of particles simultaneously. Most types of conventional position sensitive, proportional detectors with projective readout will not be able to unravel the multitude of tracks in these environments. For example, new proportional detectors with a cathode plane sub-divided into rows of pads underneath each anode wire [1,2] have recently been developed for high multiplicity particle detection. The pads in each row were connected together as a resistive line and each pad row was implemented with its own electronic readout. The sub-division of the cathode into rows with independent readout is the crucial factor in attaining both a high multiplicity capability and a higher counting rate capability. With readout nodes appropriately spaced along the pad row, resistive charge division between pads enables the position of a track along the anode wire to be determined. While this form of encoding can yield very linear position information, and can provide reasonable position resolution, formation of a resistive connection between pads requires special techniques, which are not always convenient, or even possible, when very large area detectors are involved. The use of pads with specific geometric shapes is a suitable alternative which has recently been considered; this paper reports briefly on some work we have been performing on this method.

2. Geometric Cathode Pad Designs

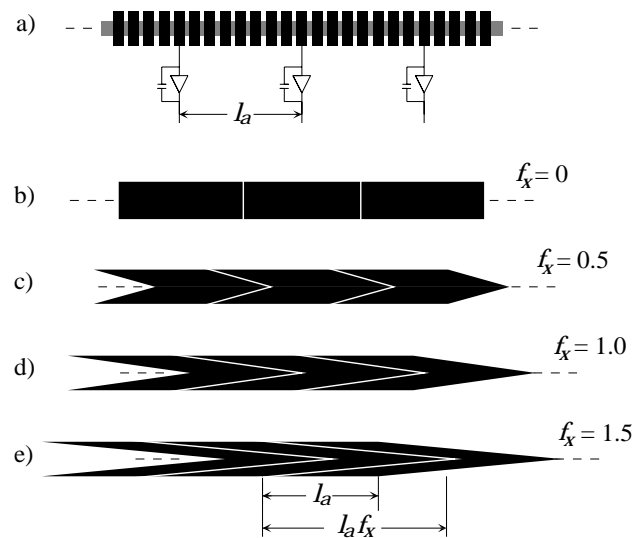


Figure.1 (a) Row of resistively coupled cathode pads, with readout every eighth pad. (b)-(e) Single chevron pads with progressively increasing depth, illustrating the definition of f_x . The readout spacing, l_a , is the same in all five examples. Anode wire position shown by dashed lines.

One of the first methods used in a gas proportional detector for position determination with geometric charge division was the 'backgammon' electrode, devised by Allemand and Thomas [3]. Several variations of this idea have been developed subsequently, for example the wedge and strip electrode [4] and diamond shaped cathode pads [5]. The principle of all these methods, however, is the same: induced cathode charge has a finite spatial extent, and the ratio of charge collected by two or more specifically shaped electrodes determines the center of gravity of the induced charge distribution. One of the major goals of the electrode design is to ensure that the measured center of gravity is as close to the real center of gravity as possible (for the present application, generally within a few tens of microns at most).

*This research was supported by the U.S. Department of Energy under Contract No. DE-AC02-76CH00016.

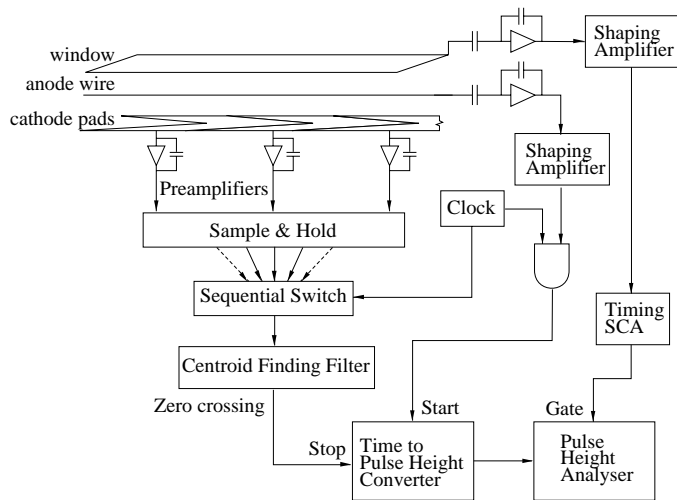


Figure 2. A section along part of the small, test detector, and the associated electronics for centroid measurements. This particular cathode shows a row of centered, single chevrons.

Fig. 1(a) shows a row of conventional, rectangular pads connected by a resistive strip, with a readout node every eighth pad. The condition that there be no modulation of the position output is that $w/d \leq 0.8$, where w is the pad pitch and d is the anode, cathode spacing. With optimized geometric charge division, one pad of a specific shape would replace the eight pads per node, and still maintain good position linearity and resolution. Similar to previous geometric charge division techniques, one of the simplest shapes for a pad is a chevron. Fig. 1(b)-(e) show chevron pad patterns with progressively increasing depth. These figures illustrate the definition of the parameter f_x . The readout node spacing, l_a , is constant in all five examples of fig. 1.

The dashed lines in fig. 1 indicate the position of the anode wire, which runs above the center of each pad row. In these particular chevron examples, the width of the chevron is equal to the anode wire pitch, s (or slightly less if guard strips are placed between pad rows [1]). The chevron apices are, furthermore, centered on the anode wire; this particular set are referred to as centered, single chevrons. More chevron geometries will be discussed in section 5.

3. Experimental Set-up

We have constructed a small test detector whose electrode spacings are the same as those used in our first large detector which used resistive charge division with pads [1]. The anode, cathode spacing, d , is 2 mm, the anode wire spacing, s , is 4 mm, and in between each anode wire is a field wire, also with a pitch of 4 mm. Cathodes with pad pitch, l_a , either 6 mm or 12 mm, were investigated. Cathode pads were 3.05 mm wide, with a 0.95 mm wide guard strip between pad rows. For our preliminary measurement purposes, the charge outputs from the cathode pads were fed into a centroid finding system [6] which operates by sequential switching of

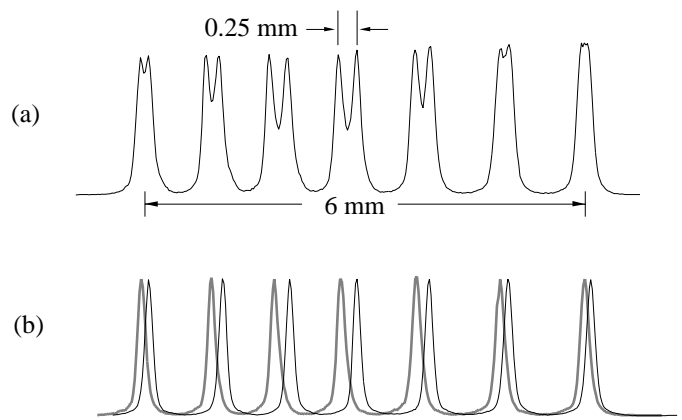


Figure 3. (a) Position spectrum from collimated X-ray scan, in 1 mm steps, from one node to the next of centered, single chevron with l_a equal to 6 mm. (b) Individual position spectra, from similar scan, for pad-side (thick line) and window-side events, which are separately selected electronically.

charge samples into a special filter. Fig. 2 shows a schematic representation along a part of one anode of the detector and the associated encoding electronics. For test purposes, a beam of X-rays, either wide enough to uniformly irradiate across several nodes, or collimated to about 15 μm , could be directed onto the detector.

4. Effects of Avalanche Angular Localization

An important characteristic of geometric charge division is that the encoded position can be very sensitive to the size of the ‘footprint’ of induced cathode charge. The shape and size of the geometric cathode pads require careful design in order to eliminate, or minimize, non-linearities due to this effect. A simple illustration of this can be seen in the results for a row of single chevrons with f_x equal to unity (fig. 1(d)), and readout spacing, l_a , 6 mm. A collimated X-ray beam was moved in 1 mm steps along the anode wire, from one node to the next, and the position response from the cathode recorded at each step. In the resulting spectrum, fig. 3(a), position peaks are split into two, with varying degrees of separation between the two peaks. An X-ray leaves a point-like deposit of ionization in the gas, and therefore it is possible to distinguish two types of event: photons that are absorbed between the anode wires and the cathode pads (pad-side events) and photons that are absorbed between the anode wires and the window (window-side events). Because of avalanche angular localization, the positive ions from the avalanches of these two types of event move in opposite directions and, depending upon the amplifier shaping time, there can be a considerable difference in the size of the induced cathode charge footprint. This is shown schematically in fig. 4. The smaller, dot-filled circle represents induced charge due to pad-side events, and the larger, hatched circle that due to window-side events. If Q_1 , Q_2 and Q_3 represent

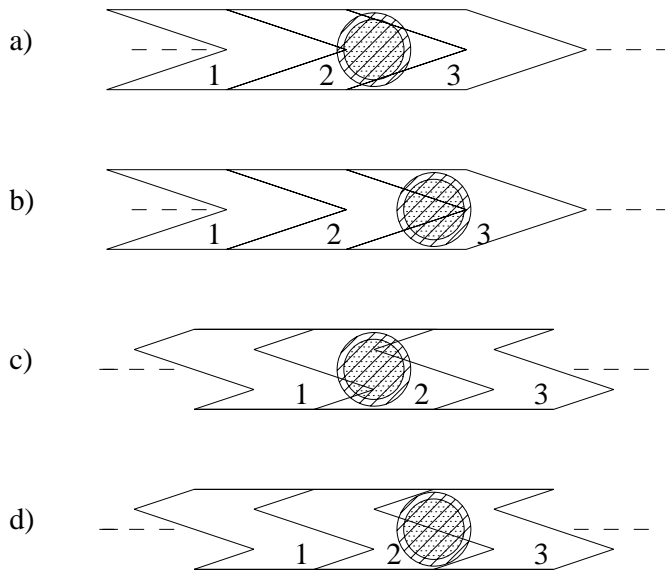


Figure 4. Schematic representation of induced charge from pad-side events (dot filled circle) and window-side (hatched circle) events. (a) shows position over a node, and (b) shows position midway between nodes, of centered single chevron. (c) and (d) are corresponding situations for displaced single chevron. Note that the actual distribution of induced charge has a quasi-Lorentzian profile with FWHM about 1.6 times the anode, cathodespacing.

the charge received by pads 1, 2 and 3 respectively, then for an event centered over node 2 (that is, centered with respect to pad-side events), fig. 4(a), Q_2 is the dominant charge. For pad-side events, $Q_1 = Q_3$, while for window-side events Q_1 is just less than Q_3 , resulting in a small displacement to the right for window-side events. Midway between nodes, fig. 4(b), induced charge is shared nearly equally between pads 2 and 3; however, there is a significantly greater difference between Q_2 and Q_3 for window-side events than for pad-side events, accounting for the greater displacement of the two events between nodes. In this particular example the separation reaches a maximum of about $250 \mu\text{m}$ exactly mid-way between nodes.

The nature of the induced signal on the window of the detector is also different for pad-side events compared to window-side events. By using an appropriate filter and analyzer it is possible to select independently each event type [7] and apply a gating signal to the analysis of position signals, as shown in fig. 2. The two resulting position spectra are shown in fig. 4(b), with position peaks well resolved.

The measured separation of pad- and window-side events can be largely eliminated by shifting the chevron pattern by one half of a chevron width. Over a node, and between nodes, there will be no displacement between these two types of event; fig. 4(c) and (d) show representations of induced charge for these situations. The anode wire now passes midway between the chevron apices, and these pads are referred to as displaced, single chevrons.

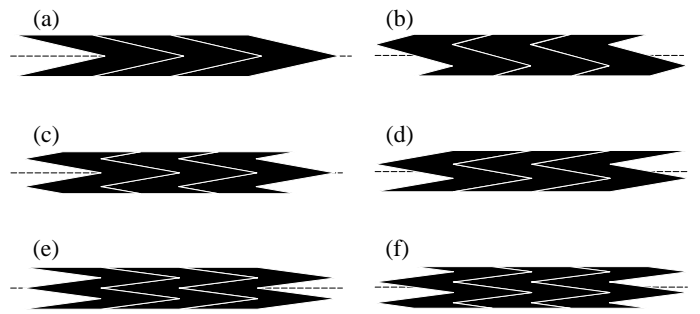


Figure 5. Patterns of (a) Centered single chevron, (b) displaced single chevron, (c) centered one & a half chevron, (d) displaced one & a half chevron, (e) centered double chevron, and (f) displaced double chevron. Dashed lines indicate anode wire positions.

Another effect can occur with geometric charge division, also due to angular localization. When a photon is absorbed to the side of the anode wire, the positive ion cloud from the resulting avalanche initially moves sideways from the anode wire; the induced cathode charge is then shifted slightly from the central axis of the pads, and a shift in the measured centroid will occur relative to an event over the anode wire. This effect results in an encoded position whose error is similar in magnitude to the separation between window and pad side events.

5. Non-linearity Measurements

Perhaps of greater importance than non-linearities due to effects of angular localization is the overall non-linearity of a specific chevron pad. This is most easily measured by uniformly irradiating a section of several pads underneath one anode wire and analyzing the position spectrum. A set of non-linearity measurements has been performed on centered and displaced versions of single chevrons, one & a half chevrons, and double chevrons with node spacing, l_a , of 12 mm; as we will see, the single chevrons do not generally provide adequate linearity, which is the reason for investigating more complex patterns. Fig. 5(a)-(f) show these chevron patterns. The corresponding differential non-linearities are illustrated in fig. 6(a)-(f), where the continuous curves show predicted non-linearity, using a best fit Gaussian for the induced cathode charge profile. The open circles represent the measurements that have been performed to date. (Differential non-linearity is defined as $(I_{\max} - I_{\min}) / ((I_{\max} + I_{\min}) / 2)$, where I_{\max} and I_{\min} are, respectively, the maximum and minimum heights in the uniform irradiation response (see next section)).

Some general characteristics are clear from fig. 6. The displaced chevron is always more linear than its corresponding, centered counterpart. Theoretically, a minimum in non-linearity is achieved for all chevron types with a value of f_x close to unity. Experimentally, the minimum non-linearity is observed with a value of f_x close to 1.05. The main reason

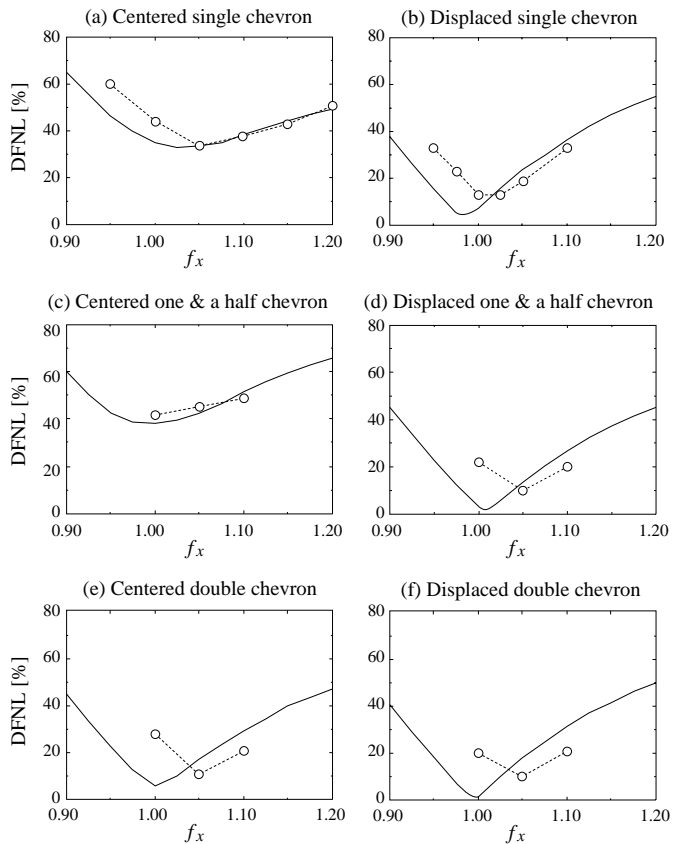


Figure 6. Differential non-linearity (DFNL) vs. f_x for (a) Centered single chevron, (b) displaced single chevron, (c) centered one & a half chevron, (d) displaced one & a half chevron, (e) centered double chevron, and (f) displaced double chevron. Readout node spacing, l_a , is 12 mm. Continuous line is the theoretical prediction, and open circles are experimental measurements.

for this small difference is due to the finite gap that must exist between adjacent pads on a real cathode board; the theory assumes that this gap is zero. Furthermore, if the gap between pads is excessively large, the non-linearity for a particular chevron type rapidly deteriorates. The displacement effects due to angular localization are, in general, negligible for the one & a half, and double chevrons, and they both exhibit a minimum differential non-linearity of $\pm 5\%$ with f_x of 1.05. Since the sharper angle of the double chevron puts greater demands on the printed circuit fabrication process, the displaced one & a half chevron is the most suitable alternative to resistively coupled pads for the present application. More detailed measurements on the small angular localization effects with this pattern are described in ref. [8].

It is interesting to observe the nature of the uniform irradiation response near minimum non-linearity. Fig. 7(a)-(c) shows the uniform irradiation spectra, over four nodes, of the displaced one & a half chevron for three values of f_x close to minimum non-linearity. Note that the phase of the modulation changes by 180 degrees in going through the minimum; this occurs for all chevrons and is also theoretically predicted.

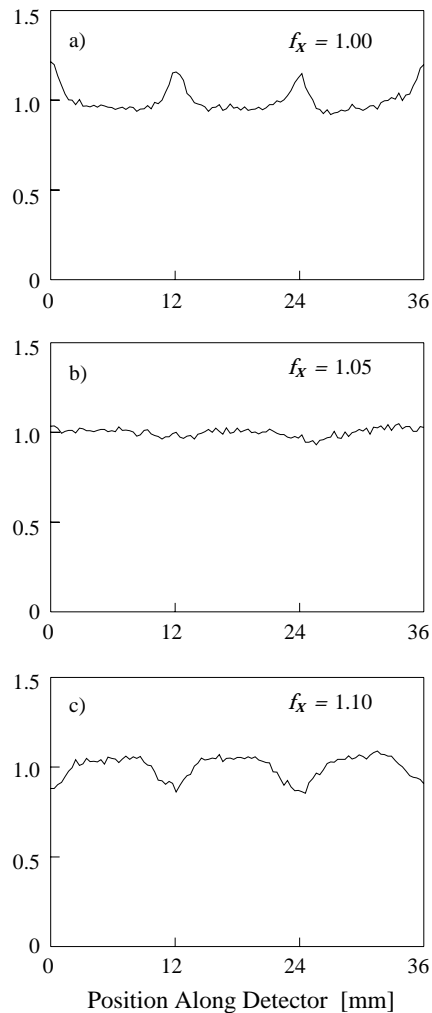


Figure 7. Uniform irradiation response, over four nodes, of displaced one & a half chevron for f_x values of (a) 1.0, (b) 1.05 and (c) 1.1. Node spacing, l_a , is 12 mm, with first node at origin of abscissa.

6. Discussion

There are some significant points that have been learned from this work regarding chevron shaped cathode pads:

a) The position of the anode wire with respect to the chevron apices is most important. The displaced chevron always yields significantly improved non-linearity compared to its centered counterpart.

b) In the geometry we have investigated, a single chevron does not usually possess enough interpolative power to eliminate centroid shift due to angular localization effects.

c) Minimum differential non-linearity with the chevron patterns used in this work occurs, theoretically, with the depth parameter, f_x , close to unity. In practice, minimum differential non-linearity is usually obtained with f_x close to 1.05. The gap between chevrons is critical in this respect. We have

achieved gaps of order 50-60 μm with standard etching techniques; with gaps of 100 μm or greater, non-linearity rapidly degrades.

d) The measurements presented here are for amplifier shaping times of approximately 1 μs , and a gas mixture of Ar/20%CO₂; smaller shaping times will reduce angular localization effects, but will not improve the global non-linearity. Measurements with particles, for which these detectors are primarily intended, will probably be less sensitive to angular localization effects than those with X-rays because of a particle's extended path of ionization. We shall follow up this work with accurate measurements using charged particles.

e) Position resolution of about 50 μm rms for 5.4 keV X-rays in Ar/20%CO₂ has been measured with these chevron pads [8]. In general, position resolution of approximately 1% of the readout spacing should be expected. Geometric charge division has the advantage over resistive charge division of having no thermal noise contribution. Capacitance between pads which have much larger readout spacing than used in this work may be a concern with respect to preamplifier noise.

f) There is considerable flexibility in the readout node spacing. Our measurements so far have been restricted to l_a values of 6 mm and 12 mm. Other applications, in which position resolution requirements may be relaxed, could incorporate much larger readout spacings. While position linearity along the major length of the chevron will still be good, it is likely that non-linearity for tracks near the apices of these chevrons would become much more sensitive to gap width, and optimization of f_x and pad shape would require re-evaluation.

Acknowledgments

The authors would like to acknowledge the skillful assistance of Ron Angona and Pat Borello in the production of printed circuit boards containing the chevron pads. Gene Von Achen carefully fabricated and assembled the remaining parts of the test detector.

References

1. R. Debbe, J. Fischer, D. Lissauer, T. Ludlam, D. Makowiecki, E. O'Brien, V. Radeka, S. Rescia, L.C. Rogers, G.C. Smith, D. Stephani, B. Yu, S.V. Greene, T.K. Hemmick, J.T. Mitchell and B. Shivakumar, *IEEE Trans. Nucl. Sci.* NS-37 (1990) 88-94.
2. A.L.S. Angels, H. Beker, J.C. Berset, G. Di Tore, C.W. Fabjan, U. Goerlach, C. Leroy, M. Price, V. Radeka, B. Sellden, V. Cherniatin and W.J. Willis, *Nucl. Instrum. & Meth.* A283 (1989) 762-766.
3. R. Allemand and G. Thomas, *Nucl. Instrum. & Meth.* 137 (1976) 141-149.
4. C. Martin, P. Jelinsky, M. Lampton, R.F. Malina and H.O. Anger, *Rev. Sci. Instrum.* 52 (1981) 1067-1074.
5. J. Allison, R.J. Barlow, R. Canas, I.P. Duerdoth, F.K. Loebinger, A.A. Macbeth, P.G. Murphy and K. Stephens, *Nucl. Instrum. & Meth.* A236 (1985) 284-288.
6. V. Radeka and R.A. Boie, *Nucl. Instrum. & Meth.* 178 (1980) 543-554.
7. G.C. Smith, J. Fischer and V. Radeka, *IEEE Trans. Nucl. Sci.* NS-31 (1984) 111-115.
8. B. Yu, G.C. Smith, V. Radeka and E. Mathieson, *IEEE Trans. Nucl. Sci.* NS-38 (1991) 454-460.